

AUSTRALIAN RADIATION PROTECTION AND NUCLEAR SAFETY AGENCY

Monte Carlo Methods used to develop
the Australian Absorbed Dose Standard

by

Keith N Wise

Technical Report 132
ISSN 0157-1400
July 2001

LOWER PLENTY ROAD
YALLAMBIE VIC. 3085
TELEPHONE: +61 3 9433 2211
FAX: +61 3 9432 1835

© Commonwealth of Australia 2001

Copyright Notice and Disclaimer

This work is copyright to the Commonwealth of Australia through the Australian Radiation Protection and Nuclear Safety Agency ('ARPANSA'). You may copy, reproduce, display and print this material in unaltered form only (retaining this notice) for your personal, research or other non-commercial use or use within your organisation, but it must not be sold for commercial gain. All other rights are reserved, apart from any use as permitted under the *Copyright Act 1968*. Requests and inquiries concerning reproduction and rights should be addressed to the Information Officer, Australian Radiation Protection and Nuclear Safety Agency, Lower Plenty Road, Yallambie, Victoria 3085.

All care has been taken in the preparation of this work and its conclusions. However, where the data or results presented are utilised by third parties outside of any intended purpose of this work, ARPANSA or the Commonwealth of Australia shall not be liable for any special, indirect, consequential or other damages whatsoever resulting from such use. Nor will ARPANSA or the Commonwealth of Australia be liable for any damages arising from or in connection with any errors or omissions that have inadvertently occurred in this work.

ABSTRACT

This report discusses the modelling strategies for the development of the Australian absorbed dose standard for high-energy photon beams via two different methods. Monte Carlo models based on the BEAM code were used to simulate all sources and physical devices. These sources include a high dose-rate cobalt-60 irradiator and the high-energy (13 - 19 MeV) radiation beams produced by the ARPANSA linear accelerator. The devices modelled include a graphite calorimeter, its associated graphite phantom and the water phantom used for the calibration of ionization chambers. Implementation of the absorbed dose standard required the calculation of physical quantities from the photon spectra for each source, including the energy-fluence weighted mass-energy absorption coefficients and the restricted stopping power ratios for graphite, water and perspex. Appendices describe the radiation sources, the calorimeter and the graphite phantom. An appendix discusses the statistical methods for the determination of the source position needed for one of the measurement methods.

CONTENTS

Page

1. INTRODUCTION.....	1
2. DETERMINATION OF D_w	3
2.1. The absorbed dose to graphite standard.....	3
2.2. Measurement of absorbed dose to water.....	4
2.3. The <i>dr</i> method.....	5
2.4. The <i>cit</i> method.....	7
3. SIMULATION STUDIES.....	10
3.1. Radiation sources.....	10
3.1.1. <i>Cobalt-60</i> source.....	10
3.1.2. <i>Linear accelerator</i> sources.....	12
3.2. Physical data.....	13
3.2.1. <i>Estimating the fluence spectra</i>	13
3.2.2. <i>Mass-energy absorption coefficients</i>	14
3.2.3. <i>Stopping power ratios</i>	14
3.2.4. <i>The ratio of calibration factors $N_{w,c}$</i>	18
4. DISCUSSION.....	19
5. REFERENCES.....	21
APPENDIX A. DETERMINATION OF THE GAP CORRECTIONS.....	A-1
A.1. The calorimeter and its phantom.....	A-1
A.2. Outline of Monte Carlo methods used.....	A-2
APPENDIX B. ESTIMATION OF VIRTUAL SOURCE POSITION.....	B-1
B.1. Statistical methods.....	B-1
B.1.1. <i>Introduction</i>	B-1
B.1.2. <i>Simple regression</i>	B-2
B.1.3. <i>Maximum likelihood</i>	B-3
B.2. Application to the ARPANSA sources.....	B-4
B.2.1. <i>Measurements with the 19MV source</i>	B-4
B.2.2. <i>Measurements with the 16MV source</i>	B-6
B.2.3. <i>Measurements with cobalt-60 source</i>	B-10

APPENDIX C. SAMPLE BEAM CODES USED IN THE SIMULATIONS.....C-1
C.1. Cobalt-60 source model.....C-1
C.2. Linear accelerator model.....C-3

INTRODUCTION

In recent years methods have been established to calibrate secondary standard ionization chambers against a primary standard for absorbed dose to water with radiation beams of energies equivalent to or higher than that of cobalt-60. For a comparison of primary standards for absorbed dose to water, see Boutillon *et al* (1994). The calibration procedure used by NPL for secondary standard dosimeters has been described by Burns and Dale (1990), by Burns (1994) and by Rosser *et al* (1994).

At ARPANSA, a secondary-standard ionization chamber (usually NE2561 or NE2611A) is calibrated against the graphite calorimeter used as the primary standard. The calibration in terms of absorbed dose to water, D_w , can be accomplished by two methods, either

- (a) directly by the “dose ratio” (*dr*) method using measurements with the water-proofed chamber in a water phantom to derive a calibration factor $N_w = D_w / Q_w$ where Q_w is the corrected charge collected, or
- (b) by the “cavity ionization theory” (*cit*) method using measurements with the chamber in a graphite phantom combined with a theoretical value for the ratio of the calibration factors for absorbed dose to water and absorbed dose to graphite, N_w / N_c

The measurement procedures to implement these steps are described in Allisy-Roberts *et al* (2000) and Boas *et al* (in preparation). As shown in Section 2, the derivation of the conversion factors requires the mass energy-absorption coefficients and, for the *cit* method only, stopping power ratios at the reference depths in water and in graphite. Data for their calculation have been tabulated in the TRS-277 protocol (IAEA 1987) supplemented by more recent data (Andreo 1994). Alternatively, computer-based methods can be applied to estimate these same quantities from models of the radiation sources used in the calibrations. Monte Carlo methods are now widely adopted for these calculations mainly because of the difficulty of measuring the spectra required to estimate the necessary physical quantities.

Several Monte Carlo codes for simulating radiation transport have been used to develop the results reported here. Initially, the *EGS4* code (Nelson *et al* 1985) was used with some comparisons being made against the *ITS3* code (Halbleib *et al* 1992). However when the *BEAM* code became available (Rogers *et al* 1995), a decision was made to standardise on this code wherever possible. This is because the *BEAM* code has been well benchmarked and tested as well as being widely adopted by the international community. The principal use for the *BEAM* code has been to calculate the photon spectra produced by the radiation sources at their collimator exits. The calculation of the particle spectra at the reference depths in water and graphite proceeds in two stages. Firstly, the geometry of the source is modelled and implemented in the *BEAM* code. Execution of the code generates a computer data file, called the phase-space data file giving the energies, positions and directions of flight for the sample of particles. Secondly, the passage of the radiation from the collimator through the phantom media is simulated by resampling the phase-space data to produce estimates of the radiation spectra at the reference depths. For this report the scoring of the photon, electron and positron fluences at the reference depths the simulations was performed with the *FLURZnrc* code from the recently implemented *EGSnrc* codes (Kawrakow 2000). A separate Fortran program performs the integrations required to estimate the mass-energy absorption coefficients and stopping power ratios.

The structure of this technical report is as follows. Section 2 presents the expressions needed for the calculation of D_w . Section 3 describes the Monte Carlo simulations and a comparison of the ratio of calibration factors $N_{w,c}=N_w/N_c$ calculated with the physical data produced for this report and with data reported elsewhere (Andreo 1994; IAEA 1987).

Throughout this paper subscripts or superscripts a , c , p and w are used to denote air, graphite, perspex and water media respectively. The ratios of some physical quantities, e.g. of mass energy-absorption coefficients or of restricted stopping powers, are used extensively and care must be taken to distinguish ratios of quantities determined at the same reference point or at different reference points. The notation X_b^a means X_a/X_b with X_a and X_b determined at different reference points while $X_{a,b}$ is the ratio of these quantities when each is determined at the same reference point.

2. DETERMINATION OF D_w

2.1. The absorbed dose to graphite standard

At ARPANSA, a Domen-type calorimeter (Domen and Lamperti 1974) is used to realise the absorbed dose to graphite at the reference point in homogeneous graphite. The ARPANSA calorimeter was constructed in 1991 by the Österreichisches Forschungszentrum (ÖFS) as described by Witzani *et al* (1984). The dose to graphite at the reference point is given by

$$D_c = (E/m) \prod_i c_k i \quad (1)$$

where E is the radiation energy absorbed in the core,
 m the effective graphite mass of the calorimeter core and
 $\prod_i c_k i$ the product of the correction factors required to convert the absorbed dose to graphite as measured by the calorimeter to the absorbed dose to graphite at the reference point in a homogeneous phantom.

The value of E is obtained through the electrical calibration of the calorimeters and is traceable to the respective national standards of voltage and resistance. The ARPANSA calorimeter is normally operated in the quasi-isothermal mode described by Witzani *et al* (1984). This is sometimes referred to as the heat flow mode (Huntley 1984) because the electrical power input to the various bodies is adjusted so that heat flows from the core to the surrounding bodies. The electrical power input is adjusted to approximately match the anticipated radiation power, so that only small changes in temperature occur if the electrical power is switched off during the irradiation period. These small temperature changes can be readily monitored and related to the difference between electrical and radiation power inputs.

The physical constants, corrections factors and uncertainties are discussed in Boas *et al* (in preparation). An important correction is that for the presence of vacuum gaps around the core of the calorimeter. This correction has been derived by the Monte Carlo methods discussed in Appendix A.

2.2. Measurement of absorbed dose to water

At ARPANSA the absorbed dose to water is derived from a calorimetric determination of the absorbed dose to graphite by two distinct methods known as the dose ratio (*dr*) and the cavity ionisation theory (*cit*) methods. In the *dr* method, use is made of the photon-fluence scaling theorem (Pruitt and Loevinger 1982) to determine the ratio of photon fluences at each reference point in graphite and in water. In the *cit* method, the cavity of the ionisation chamber is treated as a Bragg-Gray cavity with the ionisation chamber acting as an electron detector. Indirect use is also made of the photon fluence scaling theorem to ensure that the ratio of primary to scattered radiation and shapes of the radiation spectra are similar at the two reference points. Two distinct relations are used to define the dose at the reference point in the undisturbed medium.

If transient charged particle equilibrium is assumed to hold then the dose to the undisturbed medium m is related to the photon fluence by

$$D_m = \psi_m \overline{(\mu_{en} / \rho)}_m \beta_m \quad (2)$$

where

D_m is the absorbed dose to the medium at the reference point in the medium,

ψ_m is the photon energy fluence at the reference point in the medium,

$\overline{(\mu_{en} / \rho)}_m$ is mean mass energy-absorption coefficient of the medium for the photon energy spectra at the reference point,

β_m is the ratio of absorbed dose to the collision component of kerma at the reference point in the medium.

For an air cavity at the reference point in the medium at which the Bragg-Gray conditions (Attix 1986) hold, the dose to the undisturbed medium m is related to the dose to the air cavity by (Nahum 1994)

$$D_m = f D_a \quad (3)$$

For the cavity acting as an electron detector

$$f = [L(\Delta) / \rho]_{m,a} \quad (4)$$

where $(L(\Delta) / \rho)_{m,a}$ is the ratio of mean restricted stopping power ratios of the medium and air ($E = 10$ keV).

The *dr* method is developed from equation (2) while the *cit* method proceeds from (3) and (4). It should be noted that the National Physical Laboratory has developed their approach to the *cit* method from equation (2). However, by reason of its physical clarity, a derivation from (3) and (4) is preferred here.

2.3. The *dr* method

The *dr* method relates the dose at the reference point in graphite to that at the reference point in water. The dose at the reference point in water, D_w , is therefore calculated from the dose at the scaled reference point in graphite, D_c , obtained from the calorimeter measurement. Calibration of the ionisation chamber at the reference points in water proceeds from a relationship between the absorbed doses at the respective reference points as

$$D_w = D_c \psi_c^w (\overline{\mu_{en} / \rho})_c^w \beta_c^w \quad (5)$$

where

ψ_c^w is the ratio of the photon energy fluence at the reference points in water and in graphite,

$(\overline{\mu_{en} / \rho})_c^w$ is the ratio of mean mass energy-absorption coefficients of water and graphite for the photon energy spectra at the corresponding reference points,

β_c^w is the ratio of absorbed dose to the collision components of kerma at the reference points in the mediums (water or graphite).

The factors $(\overline{\mu_{en}}/\rho)_c^w$ and β_c^w are derived by calculation by methods such as those described in this report. ψ_c^w is determined from the photon fluence scaling theorem (Pruitt and Loevinger 1982) by scaling all phantom dimensions, depths in phantoms and distances from the source in the inverse ratio of the electron densities of water and graphite. Under these mapped conditions and provided that Compton scattering in the phantoms is the only interaction mechanism, the ratio of primary to scattered radiations will be the same at corresponding points. For a point source, the ratio of the photon fluences at these mapped reference points will be in the inverse ratio of the square of their distances from the source and hence

$$\psi_c^w = (R_c / R_w)^2 \prod_i k_i \quad (6)$$

where

R_c, R_w are the distances from the source to the reference points in graphite and water respectively, and

$\prod_i k_i$ is the product of correction factors factors such as for the attenuation by the front window of the water phantom, for the additional air attenuation between the calorimeter and water phantom positions, for the failure to scale the graphite phantom to the dimensions of the water phantom (k_{pg}) and for the small number of non-Compton interactions (k_{nc}) (Allisy-Roberts *et al* 2000).

Thus, provided that R_c, R_w and the physical constants are known, ${}_{dr}D_w$ can be calculated from D_c using (2) and (6) from

$${}_{dr}D_w = D_c (R_c/R_w)^2 (\overline{\mu_{en}}/\rho)_c^w \beta_c^w \prod_i k_i \quad (7)$$

Clearly, the conversion is dependent on accurate knowledge of the position of the radiation source. The statistical methods used to determine the position for sources used at the ARPANSA are discussed in Appendix B.

If the calibration factors are defined at the reference point in water as ${}_{dr}N_w = D_w/Q_w$, and at the reference point in graphite as $N_c = D_c/Q_c$, then, the ratio of water and graphite calibration factors ${}_{dr}N_{w,c} = {}_{dr}N_w/N_c$ is established from

$${}_{dr}N_{w,c} = \left(\frac{Q_c}{Q_w} \right) \left(\frac{R_c}{R_w} \right)^2 \left(\frac{\mu_{en}}{\rho} \right)_c^w \beta_c^w \Pi k_i$$

2.4. The *cit* method

Introduction of the ionisation chamber into medium m perturbs the electron fluences and D_m becomes

$$D_m = [L(\Delta)/\rho]_{m,a} D_a p_u \quad (8)$$

where p_u accounts for the breakdown of the strict Bragg-Gray conditions and is expressed as the product of factors accounting for the perturbing effects of the wall, the displacement of the medium from the cavity, the presence of the electrode and so on i.e. $p_u = p_{wall} p_{dis} p_{cel}$ (Nahum 1994). Ma and Nahum (1991) have shown that the Bragg-Gray relation holds well for high energy (over 1 MeV) photon beams.

Thus, for a chamber placed in water and in graphite phantoms, the ratio of the absorbed doses in the undisturbed media is

$$\frac{D_w}{D_c} = \frac{D_a}{D_a''} \cdot \frac{[L(\Delta)/\rho]_{w,a}}{[L(\Delta)/\rho]_{c,a}''} \cdot \frac{p_u}{p_u''} \quad (9)$$

where the unprimed quantities are evaluated at the reference point in water and the double primed quantities are evaluated at the reference point in graphite. For measurements made under fixed conditions $D_a = Q_m(W/e)/\rho V$ and

$$D_w = D_c \cdot \frac{Q_w}{Q_c} \cdot \frac{[L(\Delta)/\rho]_{w,a}}{[L(\Delta)/\rho]_{c,a}} \cdot \frac{[p_{wall} p_{dis} p_{cel}]}{[p_{wall} p_{dis} p_{cel}]} \quad (10)$$

Thus, the conversion is dependent on the calculation of the physical quantities in (10).

For a graphite-walled chamber in a graphite phantom $p_{wall}'' = 1$. If an argument presented by Rogers (1992) is extended to three media for the same chamber with a perspex waterproof sheath in a water phantom, then p_{wall} is approximated by

$$p_{wall} = \frac{(L(\Delta)/\rho)_{a,w}}{\sum_{m=c,p,w} \alpha_m \beta_{m,w} (\overline{\mu_{en}}/\rho)_{m,w} (L(\Delta)/\rho)_{a,m}} \quad (11)$$

where

a, c, p, w denote the air, graphite, perspex and water, respectively, and α_m are the fraction of secondary electrons originating in medium m , $m=c, p, w$ (Lempert *et al* 1983).

There are variations on (11) that generate numerically equivalent results (Almond and Svensson 1977, Rogers 1992, Nahum 1994). Usually $\beta_{m,w}$ is ignored as the ratio is very close to unity (Nahum 1994). The displacement correction p_{dis} adjusts for the change in fluence due to removal of the medium from the cavity and is calculated from (Johansson *et al* 1978)

$$p_{dis} = 1 - k r \quad (12)$$

$$p_{dis}'' = 1 - k \rho_{c,w}^e r''$$

where

k is the displacement factor given in Table 1,

r, r'' are the internal radii of the cavity in water and graphite respectively, and

$\rho_{c,w}^e$ is the ratio of the electron density in graphite to the electron density in water.

TABLE 1
Displacement factor for photon radiation

Photon energy	Displacement factor (mm chamber radius) ⁻¹
⁶⁰ Co	0.0040
5 MV	0.0040
8 MV	0.0031
16 MV	0.0024
42 MV	0.0025

From: Johansson *et al* 1978

Equation (10) can also be rewritten in the alternative and useful forms:

$${}_{cit}N_{w,c} = \frac{D_c}{Q_c} \cdot \frac{Q_w}{D_w} = \frac{[L(\Delta)/\rho]_{w,a}}{[L(\Delta)/\rho]_{c,a}} \cdot \frac{[P_{wall} P_{dis} P_{cel}]}{[P_{wall} P_{dis} P_{cel}]} \quad (13)$$

and

$${}_{cit}k_{u,Co} = \frac{N_w^u}{N_w^{Co}} = \frac{{}_{cit}N_{w,c}^u}{{}_{cit}N_{w,c}^{Co}} \cdot \frac{N_c^u}{N_c^{Co}} \quad (14)$$

where Co and u refer to the quality of the radiation being used with cobalt-60 and with the user's beam, respectively.

3. SIMULATION STUDIES

3.1. Radiation sources

3.1.1. Cobalt-60 source. Kotler (1993) has described a simplified representation of the ARPANSA cobalt-60 source. His model is based on a cylindrical geometry that uses parallel planes and concentric cylinders as shown in Figure 1. The simplified model differs from the design of the cobalt-60 source mainly at the exit collimator which is shown with a variable diameter, D in Figure 1. The diameter was chosen by matching the computed and experimental energy fluence distributions as outlined below. The geometry is easily broken into a sequence of modules required for the BEAM code (Rogers *et al* 1995) as, (a) SLABS to represent the lead shield behind the source capsule, (b) FLATFILT to represent the cobalt-60 source capsule and the surrounding tungsten, steel and lead shielding and (c) CONS3R to represent the lead collimator in front of the source capsule. The input file to BEAM describing Kotler's original model is given in Appendix C.1. Execution of the BEAM code gave sample data for the particle energies, positions and directions at the exit plane from the collimator; the data were collected in a file known as the phase-space data file to be used in later simulations involving the cobalt-60 source.

The model was checked against experimental data obtained by measuring the current at specific points in a water phantom while moving an ionization chamber stepwise radially across the beam. To generate theoretical data for the comparison, the passage of the radiation through water was simulated as described in Section 3.2.1 to estimate the radial profile of energy fluence by use of the data in the phase-space file. The experimental and simulated data were suitably normalised and compared graphically. The diameter for the final or exit collimator in the simplified geometry was varied until the full-width at half-maxima for the experimental and the simulated data matched. A comparison of the radial profiles is given in Figure 2. The final model was used to generate the data on photons and electrons exiting from the cobalt-60 source required in other simulations. Less than 1% of the particles exiting the collimator are electrons.

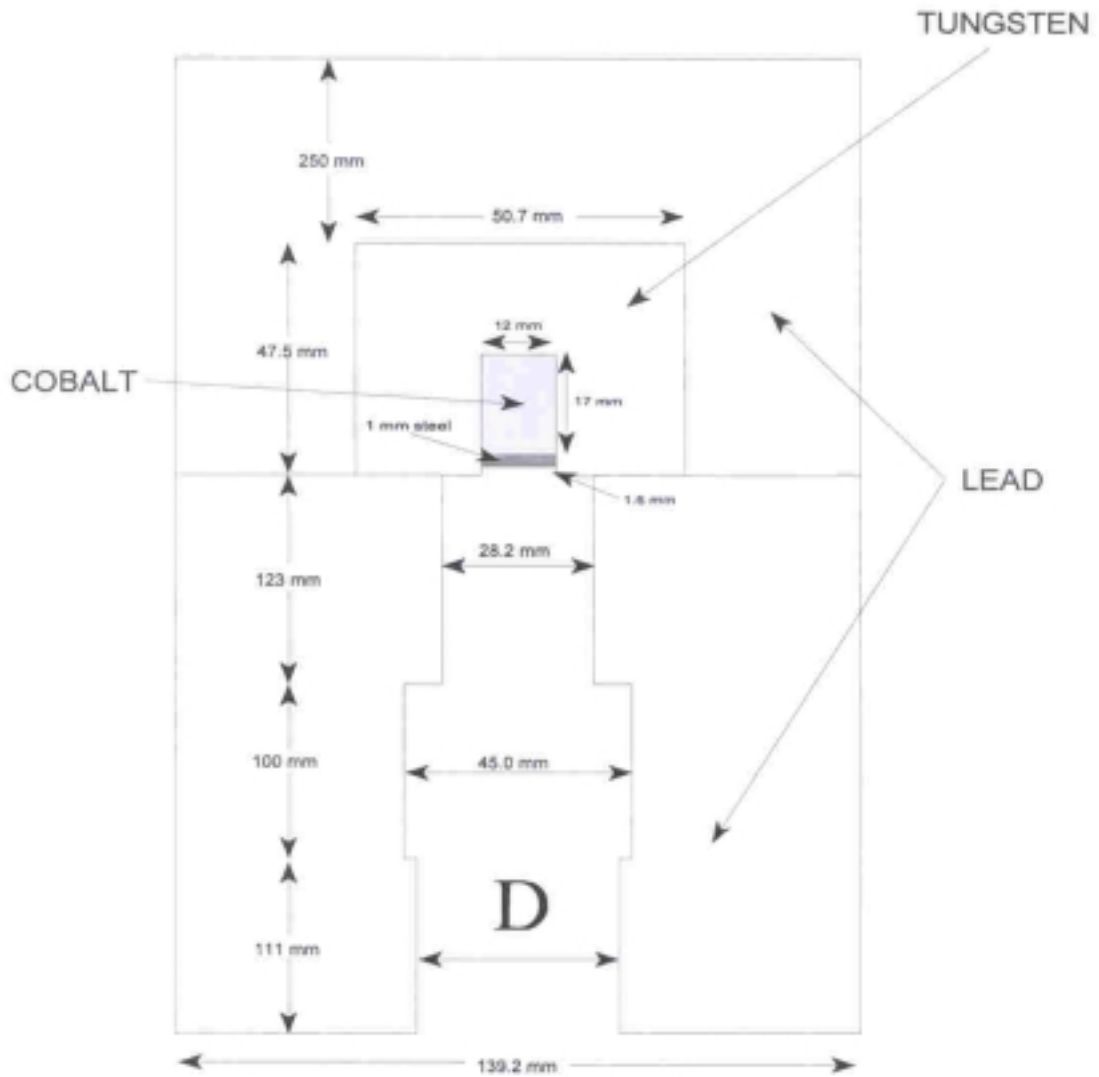


Figure I Simplified model of the ARP ANSA cobalt-60 source used in the simulations. The diameter, D , was varied to match the full width at half-maximum of the simulated and experimental profiles of absorbed dose shown in Figure 2.

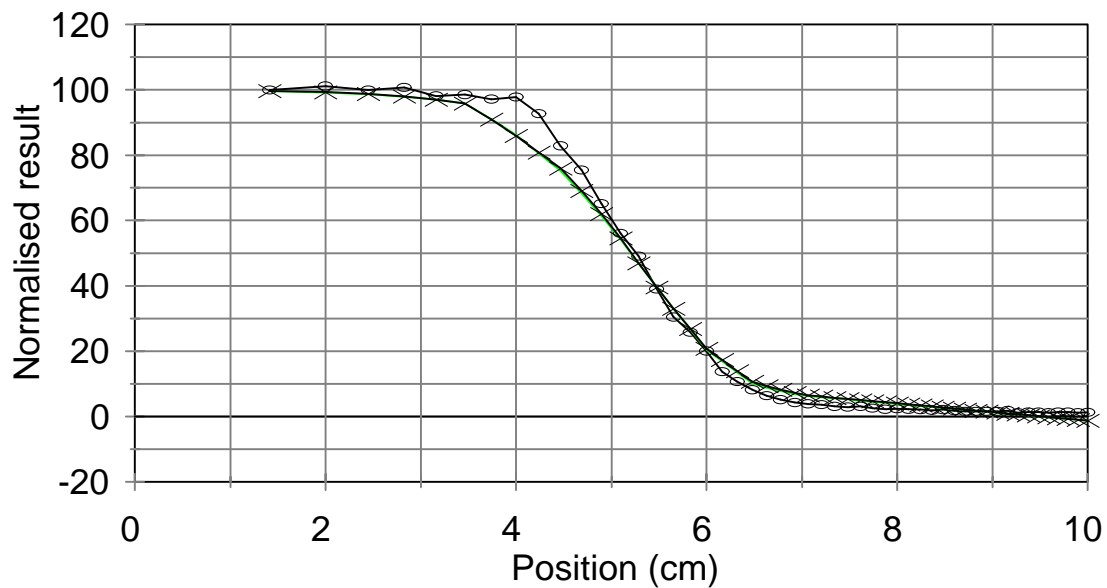


Figure 2. Comparison of the simulated radial profiles of the absorbed dose, (o), with the measured profile of the ionization current, (x), at a depth of 5cm in water. The profiles have been normalised to 100 at the smallest radial position used while the calculated profile has been chosen to match the observed full-width at half-maximum.+

3.1.2. *Linear accelerator sources.* The ARPANSA linear accelerator produces the bremsstrahlung photon spectra via electrons impacting a tantalum-aluminium target combination. The target is followed by a steel collimator containing a flattening filter, an anti-scatter ring, additional filtration and a collimation insert all of which determine the beam spectrum and its radial profile. The main BEAM modules used to implement a model of the linear accelerator are (a) SLABS to represent the titanium window and tantalum-aluminium target combination, (b) CONS3R for the primary collimator, (c) CONESTAK to describe the flattening filter, (d) CONESTAK to incorporate the anti-scatter ring, (e) CONS3R to include

additional filtration and (f) CONESTAK for the additional collimation. The input file to BEAM describing the model is given in Appendix C.2. Execution of the BEAM code gave sample data for the particle energies, positions and directions at the exit plane from the collimator collected in a phase-space data file to be used in later simulations involving the linear accelerator source.

3.2. Physical data

3.2.1. Estimating the fluence spectra. The electron, positron and photon fluence spectra were all estimated by the *EGSnrc* code *FLURZnrc*. The cylindrical geometry required by *FLURZnrc* consists of a layer of air from the collimator exit to the surface of the phantom and a cylinder of the phantom material which includes a small cylindrical region surrounding the reference point. The various distances are given in Table 2. The source particles used for transport through this slab geometry were sampled from the phase-space files. Photon spectra from the simulation were derived from the phase-space data by sorting the photon energies into bins 200keV wide. Figure 3 compares the photon spectra at the collimator exit from the cobalt-60 source and at a depth of 5cm of water. Figure 4 compares the photon spectra at 7cm of water for the 13MV, 16MV and 19MV sources modelled as described in Section 3.1.

TABLE 2
Principal distances used in the simulations

Distance	Photon beam energy	
	⁶⁰ Co	13-19 MV
Source - water, cm	105.00	275.26
Collimator – water, cm	66.42	157.09
Source - graphite, cm	65.056	170.87
Collimator - graphite, cm	28.378	52.70
Reference depth g.cm ⁻²	5.00	7.00

3.2.2. *Mass energy-absorption coefficients.* The coefficients $(\mu_{en}/\rho)_m$ are evaluated from estimates of the photon spectra at the reference depth in water and in graphite using:

$$\overline{(\mu_{en}/\rho)_m} = \frac{\int_0^{E_{\max}} \psi(E) (\mu_{en}/\rho)_m dE}{\int_0^{E_{\max}} \psi(E) dE} \quad (9)$$

where $\psi(E)$ is the differential energy fluence and $(\mu_{en}/\rho)_m$ is the mass energy-absorption coefficients from the tables of Higgins *et al* (1992). Table 3 compares the estimated coefficients against the values reported in the IAEA protocol (1987) and in Burns (1994). The significance of the various estimates of $(\mu_{en}/\rho)_m$ is discussed in Section 3.2.4.

3.2.3. *Stopping power ratios.* The calculation energy fluence ratios for equation (8) requires values for the stopping power ratios at the reference depths in water and in graphite. These may be interpolated from the stopping powers of various media relative to air given in the IAEA protocol (1987) and in Andreo (1994). The stopping power ratios for each medium relative to air were also calculated from the electron fluences estimated at the reference depths using the *FLURZnrc* code as described above from the ratio of integrals, viz.

$$(L(\Delta)/\rho)_{m,a} = \frac{\int_0^{E_{\max}} \Phi(E) (L(\Delta)/\rho)_m dE + TE_m}{\int_{\Delta}^{E_{\max}} \Phi(E) (L(\Delta)/\rho)_a dE + TE_a} \quad (10)$$

where TE_m is the track end term in medium m . The contributions of positrons to the total stopping power was also included. Data for the restricted stopping powers of the electrons and positrons was extracted using the PEGS4 data processor as described by Nelson *et al* (1985); see also Malamut *et al* 1991. Table 4 compares the estimates with those obtained by linear interpolation from the tables of the IAEA and of Andreo. The significance of the various estimates of $[L(\Delta)/\rho]_{m,a}$ is discussed in Section 3.2.4.

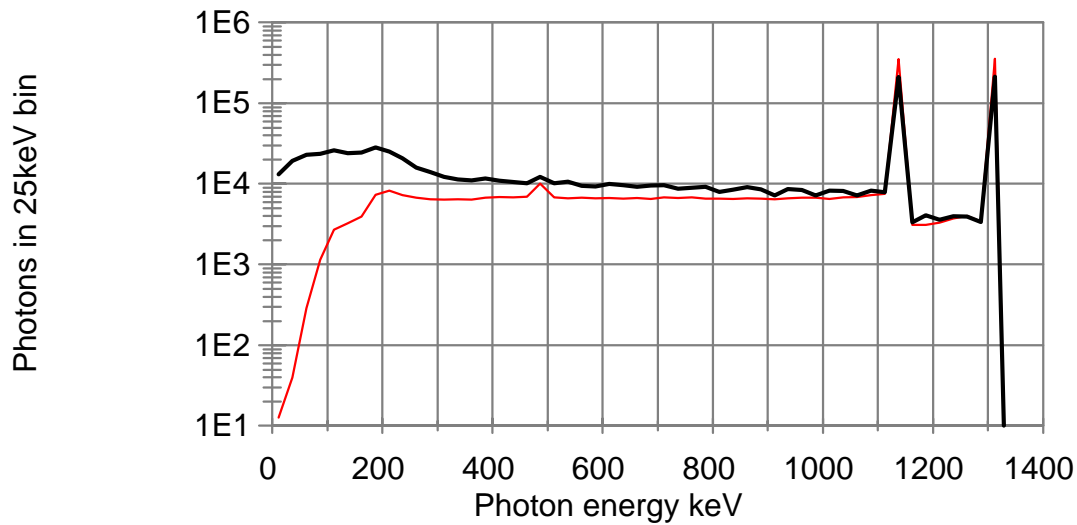


Figure 3. Photon spectra as simulated in air, (light line), and at a depth of 5cm of water, (heavy line), for the ARPANSA cobalt-60 source. The spectra have been normalised to have the same total area. The peaks are the 1.173 and 1.333 MeV gamma-rays from the decay of cobalt-60 while other photon energies arise from scatter in the source, the collimator and the intervening media.

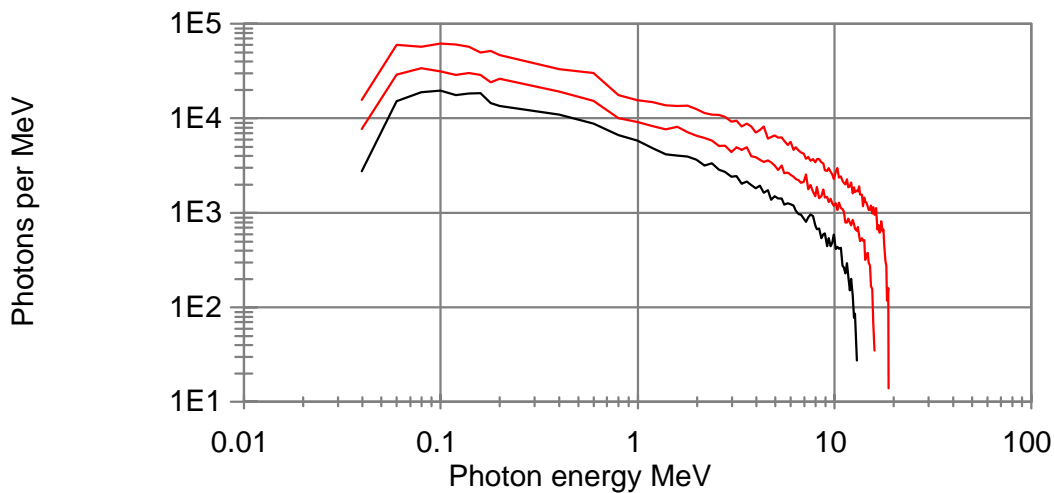


Figure 4. Photon spectra at a depth of 7cm water estimated for photon beams from linear accelerator sources at 19MV (highest line), 16MV (middle line) and 13MV (lowest line) sources. The spectra have been displaced for clarity.

TABLE 3

Comparison of mass energy-absorption coefficients

Nominal MV	TPR _{20,10}	Ratio	Mass-energy absorption coefficient		
			IAEA	NPL	ARP
Co-60	0.572	$(\mu_{en}/\rho)_c^w$	na	na	1.1136 (2)
13MV	0.763		na	na	1.1237 (4)
16MV	0.779		na	na	1.1257 (6)
19MV	0.790		na	na	1.1257 (3)
Co-60	0.572	$(\mu_{en}/\rho)_{w,c}$	1.1130	1.1110	1.1142 (<1)
13MV	0.763		1.1216	1.1238	1.1209 (<1)
16MV	0.779		1.1248	1.1265	1.1246 (<1)
19MV	0.790		1.1275	1.1284	1.1273 (<1)
Co-60	0.572	$(\mu_{en}/\rho)_{p,w}$	0.9709	0.9719	0.9700 (<1)
13MV	0.763		0.9601	0.9576	0.9619 (<1)
16MV	0.779		0.9571	0.9545	0.9579 (<1)
19MV	0.790		0.9542	0.9524	0.9550 (<1)

- Notes (1) IAEA values are from IAEA (1987), NPL values are from Burns (1994)
 ARP values have been calculated for this work.
 (2) Bracketed numbers are the standard error of the mean ratio; (2) is
 interpreted as 0.0002 and (<1) is interpreted as < 0.0001.

TABLE 4

Comparison of stopping power ratios relative to air

Beam Energy	TPR _{20,10}	Restricted stopping power relative to air			
		IAEA	Andreo	ARP	ARP''
graphite:air					
Co-60	0.5724	1.0018	1.0028	1.0009 (1)	1.0008 (4)
13MV	0.763	0.9658	0.9618	0.9623 (5)	0.9619 (4)
16MV	0.778	0.9598	0.9558	0.9527 (6)	0.9532 (4)
19MV	0.790	0.9545	0.9510	0.9467 (5)	0.9479 (6)
perspex:air					
Co-60	0.5724	1.1008	1.1012	1.1009 (<1)	1.1008 (2)
13MV	0.763	1.0647	1.0617	1.0622 (6)	1.0619 (4)
16MV	0.778	1.0579	1.0549	1.0516 (7)	1.0521 (4)
19MV	0.790	1.0520	1.0495	1.0449 (5)	1.0463 (7)
water:air					
Co-60	0.5724	1.1312	1.1326	1.1326 (<1)	1.1325 (2)
13MV	0.763	1.0977	1.0948	1.0964 (6)	1.0961 (4)
16MV	0.778	1.0909	1.0888	1.0857 (7)	1.0862 (4)
19MV	0.790	1.0850	1.0830	1.0788(5)	1.0804 (7)

Notes: 1. ARP values are based on the electron and positron fluences at the reference point in water while the ARP'' values are based on the fluences at the reference point in graphite.

2. bracketed numbers are the standard error of the mean restricted stopping power ratio; (2) is interpreted as 0.0002

3.2.4. *The ratio of calibration factors $N_{w,c}$.* The ratio of calibration factors, $N_{w,c} = N_w/N_c$ was calculated from the ARPANSA data in Table 2 and Table 3. These estimates were compared with values calculated from the mass-energy absorption coefficient data in IAEA (1987) and the stopping power ratios given by Andreo (1994). Both estimates for $N_{w,c}$ are given in Table 5.

The uncertainties of the ratios in Table 5 of N_w/N_c in equation (13) were derived by simulation. It was assumed that the relative uncertainties in $(\mu_{en}/\rho)_{m,w}$ and $[L(\Delta)/\rho]_{m,a}$ given respectively by IAEA (1987) and by Andreo (1994) for each medium, m , correspond to 0.2% and 0.3%. Data given in Table A.14.3 of Burns and Dale (1990) for the ionization fraction, α , for a range of wall thicknesses, w , and $TPR_{20,10}$ values were used to fit α to $a_0 + a_1 \cdot \log_e(w)$ at each value of $TPR_{20,10}$. The regression analysis provided estimates for a_0 , a_1 and their correlation coefficient. 100 independent values were sampled for each $(\mu_{en}/\rho)_{m,w}$ and $[L(\Delta)/\rho]_{m,a}$. Samples of 100 pairs of values for a_0 and a_1 were also created to derive estimates for α_c , α_p and α_w based on a graphite wall thickness of $0.09\text{g}\cdot\text{cm}^{-2}$ and a perspex sheath thickness of $0.18\text{g}\cdot\text{cm}^{-2}$. Finally, a random sample of the ratios p_{dis} / p_{dis}'' was constructed from the expressions in (12) for a chamber with internal radius of 3.7mm assuming an uncertainty of 10% in the values of k in Table 1. N_w/N_c was then calculated from (10) and (11) for each sample. The mean, standard deviation and relative uncertainty of N_w/N_c was then estimated. The simulations showed the relative uncertainties to be 0.2% for the cobalt-60 beam and 0.3% for the high energy beams.

TABLE 5

Estimates of N_w/N_c

Photon beam energy	Perturbation factors			$\frac{[L(\Delta)/\rho]_{w,a}}{[L(\Delta)/\rho]_{c,a}}$	N_w/N_c
	p_{wall}	$\frac{P_{dis}}{P_{dis}}$	$\frac{P_{wall} P_{dis}}{P_{dis}}$		
ARPANSA					
Co-60	0.9916	1.0093	1.0008	1.1317	1.1326
13 MV	0.9983	1.0064	1.0046	1.1398	1.1451
16 MV	0.9996	1.0055	1.0052	1.1390	1.1449
19 MV	1.0005	1.0055	1.0060	1.1382	1.1451
IAEA(1987) and Andreo (1984)					
Co-60	0.9920	1.0093	1.0013	1.1294	1.1309
13 MV	0.9991	1.0064	1.0064	1.1383	1.1455
16 MV	0.9999	1.0055	1.0054	1.1392	1.1453
19 MV	1.0008	1.0055	1.0064	1.1388	1.1461

4. DISCUSSION

The present report presents the methods currently used to support the development of the absorbed dose standard. Extensive use has been made of the photon fluence scaling theorem (Pruitt and Loevinger 1982) either directly in the application of the *dr* method or indirectly to ensure very similar photon and particle spectra at the reference depths in the graphite and water phantoms for the *cit* method.

Extensive simulations have been undertaken to check the validity of the photon fluence scaling theorem (*pfst*) for the ^{60}Co to 16MV photon beams. This was to ensure that no significant

corrections were needed for departures from the *pfst* as a result of non-Compton interactions. The method used was to define the position of the phantoms precisely relative to a point source in accord with the premises of the *pfst*. The diameter of the beam at the front face of the water phantom was equivalent to 100cm^2 . The energy fluences were calculated at the reference point in water and in graphite. For the ^{60}Co to 16MV photon beams the ratio of the energy fluences departed from the value expected by the *pfst* by no more than 0.05%. An additional set of simulations were undertaken for the 16MV source to check the effect of allowing the position of the graphite phantom to vary from the ideal position by $\pm 2\text{cm}$ and $\pm 10\text{cm}$. The ratios of the energy fluences per unit of incident fluence departed from their expected values by 0.1% at $\pm 2\text{cm}$ and 0.2% at $\pm 10\text{cm}$. The implication of this result is that while no additional correction is needed for any departures from the *pfst*, use of the *dr* method to determine the dose to water via equation (7) will be sensitive to any inaccuracy in the distances to the phantoms. While many measurements can be accumulated to determine the position of the virtual source for the ^{60}Co beam, as shown in Appendix B, this is not possible for the linear accelerator beams which may be subject to variation of the position of the virtual source with beam cycle. The *cit* method is not subject to these uncertainties as the use of the *pfst* is limited to ensuring that the photon and electron spectra are similar at the reference points. Hence at ARPANSA, the *dr* method is applied for calibrations with the ^{60}Co source and the *cit* method for calibrations with the linear accelerator sources.

The present report has been restricted to considering photon beams in use at ARPANSA. For photon beams of other energies, the mass-energy absorption coefficients from IAEA (1987) and the stopping power ratios from Andreo (1994) can be used to determine the absorbed dose to water using the *cit* method.

5. REFERENCES

Allisy-Roberts P, Burns D T, Boas J F, Huntley R B and Wise K N. *Comparison of the standards of absorbed dose to water of the ARPANSA and the BIPM for ^{60}Co gamma radiation. Rapport BIPM-99/17, 2000.*

Almond P R and Svensson H. *Ionization chamber dosimetry for photon and electron beams: theoretical considerations. Acta Radiologica, Therapy, Physics and Biology* **16**, 177-186, 1977.

Andreo, P. *Improved calculations of stopping power ratios and their correlation with the quality of therapeutic photon beams.* IN “Measurement Assurance in Dosimetry”, IAEA, Vienna, pp335-359, 1994.

Attix F H. *Introduction to radiological physics and radiation dosimetry.* John Wiley and Sons, New York 1986.

Boas J F, Duane S, Huntley R B, Rosser K, Stoker I, Thomas R, Webb D V and Wise K N. *A comparison of the absorbed dose standards for ^{60}Co and MV radiations.* (in preparation)

Boutillon M. *Gap correction for the calorimetric measurement of absorbed dose in graphite with a ^{60}Co beam.* Phys Med Biol **34**, 1809-1821, 1989.

Boutillon M, Coursey B M, Hohlfield K, Owen B and Rogers D W O. *Comparison of primary water absorbed dose standards.* IN “Measurement Assurance in Dosimetry”, IAEA, Vienna, pp95-111, 1994.

Burns J E. *Absorbed-dose calibrations in high-energy photon beams at the National physical Laboratory: conversion procedure.* Phys. Med. Biol. **39**, 1555-1575, 1994.

Burns J E and Dale J W G. *Conversion of absorbed-dose calibration from graphite into water.* National Physical Laboratory Report RSA(EXT) 7, 1990.

Cox D R and Hinkley D V. *Theoretical Statistics.* Chapman and Hall, London, 1974.

Dobson A J. *An introduction to generalized linear models*. Chapman and Hall, London, 1990.

Domen S J and Lamperti P J. *A heat-loss compensated calorimeter: theory, design and performance*. J Res Bur Stds **78A**, 595- 610, 1974.

Halbleib J A, Kensek R P, Valdez G, Seltzer S M and Berger M J. *ITS Version 3.0: the integrated TIGER series of coupled electron/photon Monte Carlo transport codes*. Sandia National Laboratories Report 91-1643, 1992.

Higgins P D, Attix F H, Hubbell J H, Seltzer S M, Berger M J and Sibata C H. *Mass energy-transfer and mass energy-absorption coefficients, including in-flight positron annihilation for photon energies 1keV to 100MeV*. National Institute of Standards and Technology Report NISTIR-4812, Gaithersburg, 1992. For current NIST estimates of the coefficients see: <http://physics.nist.gov/PhysRefData/XrayMassCoef/cover.html>

Huntley R B 1984 *A graphite microcalorimeter as a working standard of ionising radiation absorbed dose*. MSc Thesis, Royal Melbourne Institute of Technology.

International Atomic Energy Agency. *Absorbed dose determination in photon and electron beams*. Technical Report Series 277, Vienna, 1987.

Johansson K-A, Mattson L O, Lindborg L and Svensson H. *Absorbed-dose determination with ionization chambers in electron and photon beams having energies between 1 and 50MeV*. IN "National and International Standardization of Radiation Dosimetry", Vol II, IAEA, Vienna, pp243-269, 1978.

Kawrakow I. *EGSnrc, the new EGS4 version*. Med Phys **27**, 485-498, 2000.

Kotler L H 1993 *The development of a primary exposure standard for photon emission from cobalt-60 using an aluminium Kemp-Barber ionization chamber*. MSc Thesis, University of Melbourne.

Lempert G D, Nath R, Schulz R J. *Fraction of ionization from electrons arising in the wall of an ionization chamber.* Med Phys **10**, 1-3, 1983.

Ma C-M and Nahum A E. *Bragg-Gray theory and ion chamber dosimetry for photon beams.* Phys Med Biol **36**, 413-428, 1991.

Malamut C, Rogers D W O and Bielajew A F. *Calculation of water/air stopping power ratios using EGS4 with explicit treatment of electron-positron differences.* Med Phys **18**, 1222-8, 1991.

Nahum A E. *Perturbation effects in dosimetry.* Report of Joint Department of Physics, Institute of cancer Research and Royal Marsden Hospital ICR-PHYS-1/94, 1994.

Nelson W R, Hirayama H and Rogers D W O. *The EGS4 code system.* Stanford Linear Accelerator Center report SLAC-265, 1985. The code is available via the Internet at address <http://ehssun.lbl.gov/egs/egs.html>

Owen B and DuSautoy A R. *Correction for the effect of the gaps around the core of an absorbed dose graphite calorimeter in high energy photon radiation.* Phys Med Biol **36**, 1699-1704, 1991.

Pruitt J S and Loevinger R. *The photon-fluence scaling theorem for Compton scattered radiation.* Med Phys **9** 176-179 1982.

Rogers D W O. *Fundamentals of high energy x-ray and electron dosimetry protocols.* IN "Advances in radiation oncology physics, treatment planning and brachytherapy", Med Phys Monograph 19, J A Purdy (ed) AIP:New York, 1992.

Rogers D W O, Faddegon B A, Ding G X, Ma C-M and We J. *BEAM: a Monte Carlo code to simulate radiotherapy treatment units.* Med Phys **22**, 503-524,1995.

Rogers D W O, Ma C-M, Ding G X and Walters B. *BEAM Users Manual*. National Research Council of Canada Report PIRS-0509(A) rev B, 1997. The manual is available to authorized users at the Internet address <http://www.irs.inms.nrc.ca/inms/irs/BEAM/beamhome.html>

Rosser K E, Owen B, DuSautoy A R, Pritchard D H, Stoker I and Brend C J. *The NPL absorbed dose to water calibration service for high energy photons*. IN “Measurement Assurance in Dosimetry”, IAEA, Vienna, pp73-81, 1994.

SPSS Inc. *SYSTAT 6.0 for Windows*. Chicago 1996.

Witzani J, Duftschmid K E, Strachotinsky Ch and Leitner A *A graphite absorbed dose calorimeter in the quasi-isothermal mode of operation*. *Metrologia* **20** 73-79, 1984.

APPENDIX A. DETERMINATION OF THE GAP CORRECTIONS

A.1. The calorimeter and its phantom

The Australian National Standard for absorbed dose is based on a graphite calorimeter constructed by the Austrian Research Centre at Siebersdorf (ARCS) to a design of Domen and Lamperti (1974). The calorimeter measures the heating effect of the radiation beam on a graphite core, which is insulated by a number of concentric graphite shells separated by vacuum regions, by comparison with electrical heating. The calorimeter is accompanied by an almost identical graphite phantom into which ionization chambers may be inserted at a position corresponding to the centre of the core in the ARCS calorimeter thus facilitating comparison of the ionization chamber with the calorimeter. The phantom differs from the calorimeter in that the former has no vacuum gaps i.e. the phantom is essentially a solid block of graphite. Boutillon (1978) and Owen and DuSautoy (1991) have shown that for accurate work, one must correct for the slight difference in energy absorbed in the calorimeter core and an identical region in the phantom.

A.2. Outline of Monte Carlo methods used

Monte Carlo calculations of the gap corrections have been carried out for the ARCS calorimeter by estimation of the energy absorbed in the core of the calorimeter and in an identical region of the graphite phantom. These calculations used a version of the DOSRZ code which is distributed with the EGS4 package (Nelson *et al* 1985). The DOSRZ code was modified for the present application as described below. To use the code, the user's geometry needs to be reduced to a set of parallel planes and concentric cylinders and a medium assigned to each annular ring. The computer model of the ARCS calorimeter was created after simplification of the drawings for the calorimeter to a set of parallel planes and concentric cylinders. Table A.1 shows the positions of the planes relative to the centre of the calorimeter and the radii of the concentric cylinders. The annular rings are one of 4 media: vacuum, air, graphite and polyurethane. In the table, the calorimeter core is between planes at -1.375mm and 1.375mm, it has a radius of 10mm and is made of graphite (medium 2). Table A.2 shows the graphite phantom. It was created from the data in Table A.1 by filling the gap regions with graphite and ensuring that the depth of graphite to the equivalent of the calorimeter core is 30mm.

Table A.1

**Plane, radial positions and media adopted for
DOSRZ model of ARCS calorimeter**

Minimum plane (mm)	Medium to radial position (mm)											
	10	10.5	11.25	11.75	18	19	67.25	68.5	76	76.25	150	
-31.925	2	2	2	2	2	2	2	2	2	2	2	2
-6.700	2	2	2	2	2	2	2	2	3	1	2	
-4.700	0	0	0	0	0	0	2	2	3	1	2	
-4.200	2	2	2	2	2	0	2	0	3	1	2	
-3.500	0	0	0	0	2	0	2	0	3	1	2	
-2.650	2	2	2	0	2	0	2	0	3	1	2	
-1.950	0	0	2	0	2	0	2	0	3	1	2	
-1.375	2	0	2	0	2	0	2	0	3	1	2	
1.375	0	0	2	0	2	0	2	0	3	1	2	
1.950	2	2	2	0	2	0	2	0	3	1	2	
2.950	0	0	0	0	2	0	2	0	3	1	2	
3.800	2	2	2	2	2	0	2	0	3	1	2	
66.300	2	2	2	2	2	0	2	0	3	1	2	
84.600	0	0	0	0	0	0	0	0	3	1	2	
85.500	3	3	3	3	3	3	3	3	3	3	3	
95.300	1	1	1	1	1	1	1	1	1	1	1	

Notes (1) the media are vacuum=0, air=1, graphite=2, polyurethane=3
(2) the plane positions are relative to the centre of the calorimeter core

Table A.2

**Plane, radial positions and media adopted for
DOSRZ model of ARCS phantom**

Minimum plane (mm)	Medium to radial position (mm)											
	10	10.5	11.25	11.75	18	19	67.25	68.5	76	76.25	150	
-30.000	2	2	2	2	2	2	2	2	2	2	2	2
-6.700	2	2	2	2	2	2	2	2	3	1	2	2
-4.700	2	2	2	2	2	2	2	2	3	1	2	2
-4.200	2	2	2	2	2	2	2	0	3	1	2	2
-3.500	2	2	2	2	2	2	2	0	3	1	2	2
-2.650	2	2	2	2	2	2	2	0	3	1	2	2
-1.950	2	2	2	2	2	2	2	0	3	1	2	2
-1.375	2	2	2	2	2	2	2	0	3	1	2	2
1.375	2	2	2	2	2	2	2	0	3	1	2	2
1.950	2	2	2	2	2	2	2	0	3	1	2	2
2.950	2	2	2	2	2	2	2	0	3	1	2	2
3.800	2	2	2	2	2	2	2	0	3	1	2	2
66.300	2	2	2	2	2	2	2	0	3	1	2	2
84.600	2	2	2	2	2	2	0	0	3	1	2	2
85.500	3	3	3	3	3	3	3	3	3	3	3	3
95.300	1	1	1	1	1	1	1	1	1	1	1	1

Notes (1)

the media are vacuum=0, air=1, graphite=2, polyurethane=3

(2)

the plane positions have been determined from those in Table A.1 by replacing the gap regions (i.e. vacuum regions around the core) with graphite and adjusting the position of the first plane so that the distance from the centre of the core region is 30mm

Two modifications were made to the standard DOSRZ code. The first modification was introduced to improve the correlation between a calculation of the dose to the core based on the calorimeter model and the dose to the equivalent core in the phantom model. This modification ensures that the same sequence of random numbers begins the corresponding history for calculations based on two or more DOSRZ models. This is a variance reduction technique referred to as correlated sampling. The second modification introduced code to calculate the absorbed dose to the core from the mass energy-absorption coefficient for graphite, μ_{en}/ρ , times the energy fluence calculated via the sum of track lengths in the core.

The input data for DOSRZ for the calorimeter and the phantom models was prepared from the data summarised in Table A.1 and Table A.2. It was assumed that the source can be represented as a point at a given distance from the calorimeter core (or its phantom equivalent) and having identical beam radii at the core or its phantom equivalent. The data for each model included identical pairs of random numbers to drive the RANMAR random number generator which accompanies the EGS4 code. Several runs, each containing 500,000 histories were carried out with each model and the relative differences in the energy absorbed in the core calculated. The calculations were repeated several beam radii and for spectra simulated as described in Section 4.1. Table A.3 summarises the results obtained. A plot of the results, shown in Figure A.1, showed that the corrections, expressed as per-cent, could be represented by

$$\text{Gap correction}(\%) = a_E e^{-br}$$

where a_E is a constant depending only on beam energy and b is a constant. A regression analysis gave an estimate for b of 0.164 cm^{-1} and estimates for a_E for photon beams from cobalt-60, 13MV and 19MV sources of 1.402, 0.509 and 0.361, respectively.

Table A.3

Gap correction and standard error for the ARCS calorimeter as a function of radius of a ^{60}Co beam at the centre of the core

Radius (cm)	Correction \pm SE (%)		
	^{60}Co	13MV	19MV
0.350	1.278 ± 0.003	0.456 ± 0.010	0.314 ± 0.021
0.875	1.165 ± 0.007	0.439 ± 0.015	0.321 ± 0.011
1.750	1.123 ± 0.007	0.402 ± 0.012	0.267 ± 0.005
3.500	0.744 ± 0.018	0.270 ± 0.034	0.222 ± 0.015
5.250	0.555 ± 0.041	0.239 ± 0.027	0.163 ± 0.021
7.000	0.469 ± 0.050	0.188 ± 0.042	0.132 ± 0.053

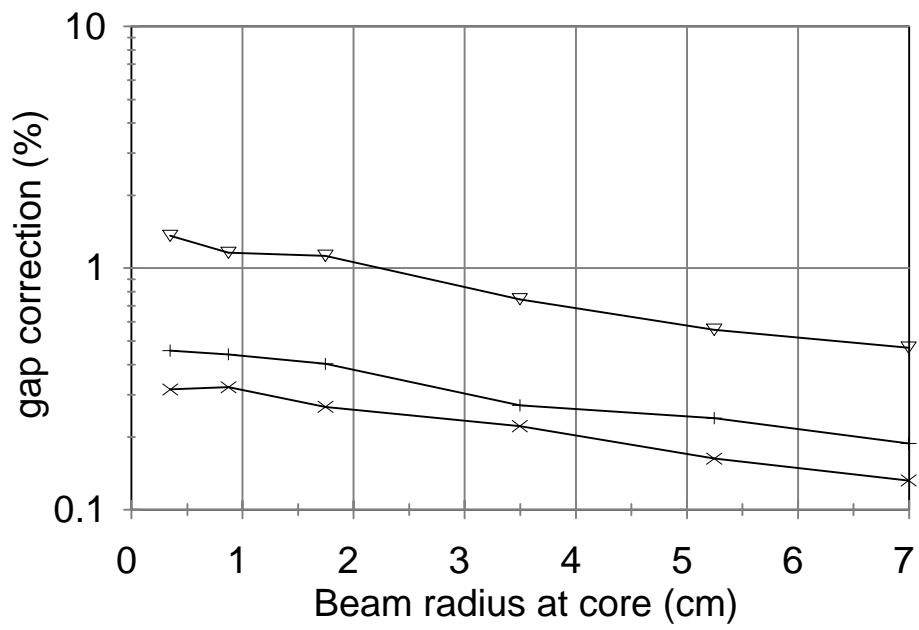


Figure A.1 Gap corrections obtained from simulations of the ARCS calorimeter with photon beams derived from the cobalt-60 (∇), 13MV (+) and 19MV radiation sources.

APPENDIX B. ESTIMATION OF VIRTUAL SOURCE POSITION

B.1. Statistical methods

B.1.1. Introduction. The application of the fluence-scaling theorem to the calculation of the calibration factors requires the radiation source to be treated as a point or virtual source. This appendix discusses methods to estimate position of the virtual source, v , relative to a reference point so that the measured air kerma or a normalized ionization chamber reading follows an inverse square law taking into account air attenuation, thus:

$$D(x) = \frac{a e^{-\mu x}}{(x + v)^2} \quad (\text{B.1})$$

where x is the distance of the chamber from a reference point.

Equation (B.1) is easily transformed from non-linear to a linear equation from which a and v and their standard errors can be estimated via conventional regression methods. However, the estimates of a and v are then biased. Other estimation techniques include generalized linear models (GLM) and the method of maximum likelihood (MML) both of which are described at an introductory level by Dobson (1990). The advantage of these methods is that the estimates are asymptotically unbiased. While (B.1) can approximate the data for a single chamber under conditions in which the radiation fluence at a point is constant over time, it is important to provide generalisations of (B.1). For example, to check that ionization chambers of the same type have identical sensitivity or to check that the virtual source position remains constant over an extended period of use of a linear accelerator. This appendix shows how the MML can be applied to generalisations of (B.1). The MML method is first applied to fit measurement data to (B.1) and then the method is extended to a more complicated example in which several ionization chambers were rotated through a number of fixed measurement points with the accelerator beam being turned off between sets of measurements.

Other fitting methods may be used for large sets of measurements. For example, the SYSTAT™ (SPSS 1996) statistical package provides tools for robust regression analysis so that unusually high or low measurement results (ie. outliers) are automatically taken into account. These tools are used below to analyse measurements made with the ARL cobalt-60 source.

B.1.2. Simple regression. Initial estimates of the parameters for use in the MML method can be obtained by rewriting (B.1) as:

$$\frac{I}{\sqrt{D(x)}} = \frac{(x e^{\mu x/2} + v e^{\mu x/2})}{\sqrt{a}}$$

or

$$I/\sqrt{D(x)} = \alpha_1 z_1 + \alpha_2 z_2 \quad (\text{B.2})$$

where $\alpha_1 = v/\sqrt{a}$, $\alpha_2 = 1/\sqrt{a}$, $z_1 = \exp(\mu x/2)$ and $z_2 = x \exp(\mu x/2)$.

Multiple regression routines are now available in many spreadsheet packages such as Excel™ and QuattroPro™ to estimate α_1, α_2 and their variance-covariance matrix from a least squares fit of $I/\sqrt{D(x)}$ to z_1, z_2 . Let $\hat{\alpha}_1, \hat{\alpha}_2$ be the estimates of α_1, α_2 with σ_1^2, σ_2^2 being the variances of α_1, α_2 and σ_{12} the covariance of α_1, α_2 then estimates of the virtual source position, v , and its standard error, s_v , are

$$\hat{v} = \hat{\alpha}_1 / \hat{\alpha}_2 \quad (\text{B.3})$$

and

$$s_v = \hat{v} \sqrt{(\sigma_1^2 / \hat{\alpha}_1^2 + \sigma_2^2 / \hat{\alpha}_2^2 - 2 \sigma_{12} / \hat{\alpha}_1 \hat{\alpha}_2)} \quad (\text{B.4})$$

SYSTAT™ provides an option, (FUNPAR), to evaluate \hat{v} and its standard error concurrently with $\hat{\alpha}_1$ and $\hat{\alpha}_2$.

B.1.3. Maximum likelihood. Given a set of n measurements, $D(x_i)$, at positions x_i , the likelihood, L , is written as the product of the n probability density functions for the measurement results. While any statistical distribution may be used, for this application the observations are assumed to be normally distributed with variance σ^2 and mean $D(x_i/a, v)$ given by

$$D(x_i/a, v) = \frac{a e^{-\mu x_i}}{(x_i + v)^2} = \hat{D}(x_i) \quad i = 1, 2, \dots, n \quad (\text{B.5})$$

The parameters a, v are estimated so as to maximise the likelihood written as the product of the

$$L(a, v, \sigma^2 / x_1, x_2, \dots, x_n) = \prod_{i=1}^n \frac{1}{\sqrt{(2\pi\sigma^2)}} \exp\left[-\frac{(D(x_i) - \hat{D}(x_i))^2}{2\sigma^2}\right]$$

n densities

An equivalent method is to estimate the parameters by minimising the log-likelihood defined as

$$\begin{aligned} \ell(a, v, \sigma^2 / x_1, x_2, \dots, x_n) &= -\log L(a, v, \sigma^2 / x_1, x_2, \dots, x_n) \\ &= \frac{n}{2} \log(2\pi\sigma^2) + \sum_{i=1}^n \frac{[D(x_i) - \hat{D}(x_i)]^2}{2\sigma^2} \end{aligned} \quad (\text{B.6})$$

The SYSTAT statistical software package was used to estimate the model parameters and their standard errors via the MML. The estimates obtained by the MML have some useful properties. While the parameters calculated via the MML are biased, the bias becomes smaller with increasing sample sizes and the distribution of the parameter estimates approaches a multivariate normal distribution. For a detailed account of the MML see Cox and Hinkley (1974).

It is straightforward to extend (B.5) to more general models. For example, for m ionization chambers, $j=1, 2, \dots, m$, measured at n positions, $i=1, 2, \dots, n$, (B.5) generalises to

$$D(x_{ij}/\vec{a}, \vec{v}, \sigma^2) = \frac{a_j e^{-\mu x_{ij}}}{(x_{ij} + v_j)^2} = \hat{D}(x_{ij}) \quad i = 1, 2, \dots, n; \quad j = 1, 2, \dots, m \quad (\text{B.7})$$

where $\vec{a} = (a_1, a_2, \dots, a_m)'$ and $\vec{v} = (v_1, v_2, \dots, v_m)'$. The improvement in the fit of the model can be checked by examining the change in the log-likelihood; in particular, the improvement in

proceeding from a model with p parameters to a model with q parameters, $q > p$, is statistically significant if $2\ell_p - 2\ell_q$ exceeds χ^2_{q-p} , i.e. a chi-square distribution for $q-p$ degrees of freedom, at an appropriate significance level.

The above models assume that the measurement results are drawn from a normal distribution with a constant variance. An alternative model that may be considered is to assume that the relative error is constant. Data analysis proceeds as described above using the logarithms of the measurement results and the mean of the distribution expressed, for example, as

$$\log D(x_i/a', v) = a' - \mu_{x_i} - 2 \log(x_i + v) \quad i = 1, 2, \dots, n \quad (\text{B.8})$$

B.1.4. Other methods. The sample sizes for the linear accelerator based studies are relatively small because of experimental limitations. However, for the investigations involving the ARL cobalt-60 source, a large series of measurements was obtained with some of the measurement results being affected by electronic noise. There are two ways of handling the unrepresentative measurement results. Either remove any unusually low or high results from the analysis after a careful inspection of the differences between the observed and expected results or robust regression to automatically reduce the importance of extreme values to the regression. The SYSTAT manual gives a useful summary on robust regression. Both approaches are used in an analysis discussed below.

B.2. Application to the ARL sources

B.2.1. Measurements with 19MV source. Measurements were made, using a single ionization chamber placed at 6 locations on the beam axis, of the ionization current per monitor unit. The 6 measurement results are shown in Table B.1. The parameter estimates in Table B.2 were obtained by regression analyses of (B.2) making no adjustment for air attenuation and including air attenuation, by the MML based on (B.5) and by the MML based on the log-transformed model (B.8). The estimates based on (B.2) show clearly the bias introduced by not including the air attenuation in the model equations.

Table B.1
Ionisation current per monitor unit

Distance (m)	Ionisation current per monitor unit
0.58162	15.25708
1.096892	8.956183
1.441095	6.700856
1.641095	5.756148
2.444183	3.431167
2.843894	2.757664

Table B.2
Parameter estimates from alternative models

Model	Estimate and standard error		
	a	$v (m)$	σ^2
(B.2) with $\mu=0$	42.719 ± 0.205	1.087 ± 0.0069	NA
(B.2) with $\mu \neq 0$	44.742 ± 0.083	1.126 ± 0.0027	NA
(B.5)	44.858 ± 0.122	1.128 ± 0.0026	1.38×10^{-5}
(B.8)	3.8026 ± 0.0042	1.127 ± 0.0052	7.18×10^{-7}

B.2.2. Measurements with 16MV source. Four ionisation chambers were placed so as to measure the ionisation current, normalised to the monitor unit reading, at 6 positions. The chambers were guided by remote control so that the 6 measurements could be completed without turning off the linear accelerator beam. The 6 positions consist of 2 fixed positions at each end with the 2 inner chambers each being able to move to either of 2 positions. The 4 chambers were rotated through the 6 positions giving a total of 24 readings. The position of the chamber was recorded as were the ionisation current per monitor unit reading corrected for recombination effects. Table B.3 summarises these measurement results. Although the mean distances and their standard deviations are given at each of the 6 positions, the actual distances recorded were used in the analysis discussed below.

Table B.3
Corrected ionisation current per monitor unit for 4 ionisation chambers

Mean distance \pm SD (mm)	Ionisation current per monitor unit for NE2561 chamber			
	194A	238A	289	328
589.25 \pm 0.58	3.10659	2.93936	2.92139	2.93145
1106.44 \pm 0.31	1.83535	1.73824	1.73647	1.73279
1506.51 \pm 0.32	1.32604	1.25058	1.24907	1.24861
2071.27 \pm 0.70	0.90292	0.84195	0.83856	0.84580
2470.85 \pm 0.60	0.71302	0.66348	0.65958	0.66580
3040.85 \pm 2.2	0.53385	0.49050	0.489299	0.48939

It is apparent from Table B.3 that one chamber (194A) is fractionally more sensitive than the other chambers. Therefore, the following sequence of models was examined to evaluate the whether the sensitivity is significantly different. Denote the 4 chambers by an index $j=1,2,3,4$ and the 6 positions by an index $i=1,2,\dots,6$. Assume that the virtual source position, v , is constant throughout the measurement program. Then (B.7) becomes

$$D(x_{ij}/\bar{a}) = \frac{a_j e^{-\mu x_{ij}}}{(x_{ij} + v)^2} \quad i = 1,2,\dots,6; \quad j = 1,2,3,4 \quad (\text{B.9})$$

This is called Model 1 for this analysis. A related model, called Model 2 here, can be created from (B.9) by assuming that 3 of the chambers, (238A, 289 and 328), are equally sensitive so that the new model distinguishes two groups by an index $j=1,2$ but is otherwise the same as (B.9). Estimates of the parameters were obtained with the SYSTAT package and are summarised in Table B.4 with Model 1 denoting (B.9) and Model 2 the simplified model. A test of whether Model 1 fits the data better than model 2 is obtained by comparing $2(\ell_4 - \ell_6) = 6.99$ with the χ^2 for 2 degrees of freedom at the 95% significance level which is 5.99. It is concluded that Model 1 does provide a significantly better fit than Model 2.

As noted above, the linear accelerator was turned off between each set of 6 measurements. Denote the virtual source position for each set by v_k , $k=1,2,3,4$. The next stage in the analysis is to test whether the fit of a model based on different v_k is significantly better than for Model 1 above. For the MML analysis write the expected result as

$$D(x_{ij}/\bar{a}, \vec{v}) = \frac{a_j e^{-\mu x_{ij}}}{(x_{ij} + v_k)^2} \quad i = 1,2,\dots,6; \quad j, k = 1,2,3,4 \quad (\text{B.10})$$

Application of the MML based on the model (B.10) gives the estimates shown in Table B.5.

A test of whether (B.10) fits the data better than Model 1 is obtained by comparing $2(\ell_6 - \ell_9) = 8.42$ with the χ^2 for 3 degrees of freedom at the 95% significance level which is 7.81. It is concluded that (B.10) provide a significantly better fit than model 1. An interpretation of this result is that virtual source position can change slightly between sets of measurements that require the linear accelerator to be turned off from set to set. From the estimates for v in Table B.5, the virtual source position can vary by about 5mm.

Table B.4
Parameter estimates for 2 models.

Model 1		Model 2	
Parameter	Estimate \pm ASE	Parameter	Estimate \pm ASE
a_1	9.3654 \pm 0.0669	a_1'	9.3656 \pm 0.0721
a_2	8.8440 \pm 0.0637	a_2'	8.8265 \pm 0.0651
a_3	8.8030 \pm 0.0635		
a_4	8.8321 \pm 0.0636		
$v(m)$	1.1435 \pm 0.0067	$v(m)$	1.1435 \pm 0.0072
σ^2	0.000020 \pm 0.000014	σ^2	0.000027 \pm 0.000017
ℓ_6	-95.513	ℓ_4	-92.017

Notes

- (1) ASE is the asymptotic standard error provided by the MML analysis
- (2) The chambers are identified by their indices. For model 1, 1=194A, 2=238A, 3=289 and 4=328. For model 2, 1=194A and 2=(238A,289 or 328).

Table B.5

Parameter estimates from equation (B.10)

Parameter	Estimate \pm ASE
a_1	9.3785 ± 0.0645
a_2	8.8417 ± 0.0616
a_3	8.8092 ± 0.0619
a_4	8.8129 ± 0.0619
$v_1 (m)$	1.1457 ± 0.0069
$v_2 (m)$	1.1449 ± 0.0067
$v_3 (m)$	1.1425 ± 0.0068
$v_4 (m)$	1.1406 ± 0.0069
2	0.000014 ± 0.000011
ℓ_9	-99.724

Notes

- (1) ASE is the asymptotic standard error provided by the MML analysis
- (2) The sensitivity parameter, a_j , for each chambers is identified by an index. For model (B.10), 1=194A, 2=238A, 3=289 and 4=328.
- (3) The virtual source position, v_k , has been estimated for each of the 4 series of measurements in which the accelerator beam was turned off between runs.

B.2.3. Measurements with cobalt-60 source. A set of over 460 measurements divided into 11 series was obtained with this source by observing the integrated current from an ionization chamber placed in a build up cap and moved along the beam axis in fixed steps under computer control. In some series of measurements the direction of movement was reversed - the measurements are therefore separated into groups where the chamber was moved either towards or away from the source. There is potential for the position of the virtual source to vary with the direction of movement due to slippage of the coupling between the drive train and the chamber holder. Preliminary analyses of the measurement results using the MML with a model similar to (B.7) showed, by inspection of the residuals normalized to the estimated standard deviation, $\hat{\sigma}$, that a number of observations were unusually high or low.

Estimates of the virtual source position were obtained using 3 methods and are summarised in Table B.7. The first 2 methods are based on the robust regression procedures in SYSTAT and in particular the TRIM option to remove 5% of the highest absolute residuals from the analysis. Model 1 was based on equation (B.2) while Model 2 was based on experience with the current integrator which showed that the variance of the integrated current is proportional to its mean (R Huntley, personal communication). Thus, Model 2 was based on a transformation of the inverse square law to

$$\sqrt{I_{ij}} = \frac{a_j' e^{-\mu x_{ij}}}{(x + v_j)} \quad (\text{B.11})$$

where I is the integrated current, i is an index for an observation and j an index for the measurement series. The third method was to use the MML with a model similar to (B.7). As the TRIM option is not available for the MML, outlier observations were removed manually. These outliers were defined to be observations which differed from those expected by the model equation by more than 3 times the estimated standard deviation, $\hat{\sigma}$.

Table B.7**Estimates of virtual source position for the cobalt-60 source by 3 methods**

Series	Direction	Virtual source position \pm standard error (mm)		
		Model 1	Model 2	Model 3
1	Away	525.91 \pm 1.09	525.69 \pm 0.98	525.47 \pm 0.25
3		524.41 \pm 1.11	524.22 \pm 0.87	524.21 \pm 0.31
4		525.36 \pm 1.15	525.03 \pm 1.13	525.70 \pm 0.22
6		524.48 \pm 0.76	524.75 \pm 0.80	524.94 \pm 0.18
8		524.94 \pm 0.46	525.05 \pm 0.35	525.20 \pm 0.21
9		524.73 \pm 0.97	526.70 \pm 0.87	527.10 \pm 0.25
11		524.51 \pm 1.05	525.21 \pm 1.04	525.60 \pm 0.23
2	Towards	529.27 \pm 1.39	524.55 \pm 1.55	523.91 \pm 0.34
5		526.88 \pm 0.73	524.35 \pm 0.87	524.01 \pm 0.23
7		526.12 \pm 1.12	524.41 \pm 1.17	524.04 \pm 0.23
10		527.37 \pm 1.12	524.82 \pm 1.27	524.10 \pm 0.24
-	Away	524.95 \pm 0.35	525.14 \pm 0.43	525.30 \pm 0.13
-	Towards	527.29 \pm 0.56	524.35 \pm 0.49	524.02 \pm 0.13

Model 1 is given by (B.2) with parameter estimates obtained as described in section B.1.2

Model 2 is given by (B.11) with parameter estimation by minimizing the sum of the squares and rejection of 5% of highest absolute residuals

Model 3 is a model similar to (B.7) with parameter estimation by the MML.

APPENDIX C. SAMPLE BEAM CODES USED IN THE SIMULATIONS

This appendix gives the input files to the BEAM code for the cobalt-60 source and the linear accelerator sources. The files are readily interpreted when read in conjunction with the BEAM manual (Rogers *et al* 1997).

C.1. Cobalt-60 source model

Model of ARL cobalt-60 source based on geometry of L H Kotler

AIR700ICRU

0, 0, 1, 0, 0, 3, 0, 0.000,

25000000, 90, 26,100.00, 1, 25, 1

0, 3, 0.00, 0.60, 27.79, 29.49,

1,

/export/home/keithw/spectra/unscat_co_60

1,

0.0, 0.0, 1.50, 0.010, 0, 1, 1.5,0,

0, 1, 1, 4, 4

2, 3, 4

4, 0,

0.5, 1.0, 1.95, 4.0

4, 0,

1.0, 2.0, 5.0, 6.96

0,

0.0000

***** start of CM slabs back of shield *****

6.9600,

Lead shield back

1

0.0

25.000, 1.50, 0.01, 0, 1, 1.0

PB700ICRU

***** start of CM flatfilt source capsule *****

7.0000,

Source capsule and shield

25.00,

4,

2, 2.79,

2.535, 6.96,

2.535, 6.96,

3, 1.70,

0.6, 2.535, 6.960,

0.6, 2.535, 6.960,

3, 0.10,

0.6, 2.535, 6.960,

0.6, 2.535, 6.960,

3, 0.16,

0.6, 2.535, 6.960,
 0.6, 2.535, 6.960,
 1.50, 0.01000, 0, 2
 W700ICRU
 1.50, 0.01000, 0, 3
 PB700ICRU
 1.50, 0.01000, 0, 20
 AIR700ICRU
 1.50, 0.01000, 0, 4
 CO700ICRU
 1.50, 0.01000, 0, 5
 W700ICRU
 1.50, 0.01000, 0, 6
 PB700ICRU
 1.50, 0.01000, 0, 20
 AIR700ICRU
 1.50, 0.01000, 0, 7
 FE700ICRU
 1.50, 0.01000, 0, 8
 W700ICRU
 1.50, 0.01000, 0, 9
 PB700ICRU
 1.50, 0.01000, 0, 20
 AIR700ICRU
 1.50, 0.01000, 0, 10
 AIR700ICRU
 1.50, 0.01000, 0, 11
 W700ICRU
 1.50, 0.01000, 0, 12
 PB700ICRU
 1.50, 0.01000, 0, 20
 AIR700ICRU
 ***** start of CM cons3r collimator *****
 6.9600,
 Primary collimator
 29.7501
 33.400
 6
 29.75, 1.41,
 42.05, 1.41,
 42.05, 2.25,
 52.05, 2.25,
 52.05, 1.62,
 63.15, 1.62,
 1.50, 0.01000, 0, 13,
 AIR700ICRU

```

1.50, 0.01000, 0, 14,
PB700ICRU
***** start of CM slabs airgap *****
6.9600,
Air gap at front
1
63.1501,
100.00, 1.50, 0.01, 0, 16, 1.0
AIR700ICRU
***** end of all CMs *****

```

C.2 Linear accelerator model

Complete model of ARL linac - Version May 1996 for 19MV accelerator

```

AIR700ICRU
0, 0, 1, 0, 0, 3, 0, 0.000,
200000, 90, 26, 24.00, 1, 32, 1
-1, 0, 0.300, 0.0, 0.0, 1.0,
0,
19.0,
0.0, 0.0, 0.70, 0.010, 0, 1, 1.0,0,
0, 1, 1, 8, 8
1, 8
5, 0,
1.0, 1.5, 2.0, 4.8, 14.0
1,
5, -1
0
3
1,
2,
3
0.0000
***** start of CM slabs target *****
6.0000,
Tantalum target
4
0.0
0.0127, 0.70, 0.01, 1, 1, 2.0
TI700ICRU
16.4, 0.70, 0.01, 2, 2, 1.0
AIR700ICRU
0.16, 0.70, 0.01, 2, 2, 1.0
TA700ICRU
6.0, 0.70, 0.01, 2, 2, 1.0

```

AL700ICRU

***** start of CM cons3r primcoll *****

14.000,

Primary collimator

22.5727

72.0

6

22.5727, 3.0

46.5727, 3.0

46.5727, 3.6

70.5727, 3.6

70.5727, 4.2

94.5727, 4.2

0.70, 0.01000, 5, 5,

AIR700ICRU

0.70, 0.01000, 6, 6

FE700ICRU

***** start of CM conestak flattenf *****

14.000,

Flattening filter

94.5727, 4.8

3

1.17, 0.46, 3.84

0.10, 4.11, 4.11

0.30, 4.565, 4.565

0.70, 0.010, 6, 6

FE700ICRU

0.70, 0.01000, 7, 7

CU700ICRU

0.70, 0.01000, 5, 5

AIR700ICRU

0.70, 0.01000, 7, 7

CU700ICRU

0.70, 0.01000, 5, 5

AIR700ICRU

0.70, 0.01000, 7, 7

CU700ICRU

0.70, 0.01000, 5, 5

AIR700ICRU

***** start of CM cons3r1 tube *****

14.000,

Primary collimator - tube

96.1427

1.0000

2

96.1427, 4.8

97.1427, 4.8

0.70, 0.01000, 5, 5,
 AIR700ICRU
 0.70, 0.01000, 6, 6
 FE700ICRU
 ***** start of CM conestak as_ring *****
 14.000,
 Anti scatter ring
 97.1427, 4.8
 1
 2.0, 3.25, 3.25
 0.70, 0.010, 6, 6
 FE700ICRU
 0.70, 0.0100, 5, 5
 AIR700ICRU
 0.70, 0.01000, 8, 8
 PB700ICRU
 ***** start of CM cons3r1 filter *****
 14.000,
 Aluminium filter
 99.1427
 3.0000
 2
 99.1427, 4.8
 102.1427, 4.8
 0.70, 0.01000, 9, 9,
 AL700ICRU
 0.70, 0.01000, 6, 6
 FE700ICRU
 ***** start of CM cons3r1 tube2 *****
 14.000,
 Primary collimator - tube2
 102.1427
 4.03
 2
 102.1427, 4.8
 106.1427, 4.8
 0.70, 0.01000, 10, 10,
 AIR700ICRU
 0.70, 0.01000, 6, 6
 FE700ICRU
 ***** start of CM conestak collim2 *****
 14.000,
 Secondary collimator
 106.1727, 4.8
 3
 4.00, 2.625, 2.625

6.00, 2.75, 2.75
2.00, 2.875, 2.875
0.70, 0.010, 6, 6
FE700ICRU
0.70, 0.01000, 10, 10
AIR700ICRU
0.70, 0.01000, 11, 11
PB700ICRU
0.70, 0.01000, 10, 10
AIR700ICRU
0.70, 0.010, 11, 11
PB700ICRU
0.70, 0.01000, 10, 10
AIR700ICRU
0.70, 0.01000, 11, 11
PB700ICRU

***** end of all CMs *****